Article

Scintica:

THE IMMUNE-METABOLIC BASIS OF EFFECTOR MEMORY **CD41 T CELL** FUNCTION UNDER HYPOXIC CONDITIONS

Sarah Dimeloe,* Matthias Mehling,*,† Corina Frick,* Jordan Loeliger,* Glenn R. Bantug,* Ursula Sauder,‡ Marco Fischer,* Re´ka Belle,* Leyla Develioglu,* Savas¸ Tay,† Anja Langenkamp,x and Christoph Hess*

g

The Journal of Immunology

The Immune-Metabolic Basis of Effector Memory CD4 + T Cell Function under Hypoxic Conditions

Sarah Dimeloe, Matthias Mehling, Corina Frick, Jordan Loeliger, Glenn R. Bantug, Ursula Sauder, Marco Fischer, Réka Belle, Leyla Develioglu, Savas Tay, Anja Langenkamp and Christoph Hess

J Immunol 2016; 196:106-114; Prepublished online 30 November 2015;
doi: 10.4049/jimmunol.1501766
http://www.jimmunol.org/content/196/1/106

The Journal of Immunology is published twice each month by
The American Association of Immunologists, Inc.,
1451 Rockville Pike, Suite 650, Rockville, MD 20852

Print ISSN: 0022-1767 Online ISSN: 1550-6606.

The Immune-Metabolic Basis of Effector Memory CD4$^+$ T Cell Function under Hypoxic Conditions

Sarah Dimeloe,* Matthias Mehling,*,† Corina Frick,* Jordan Loeliger,* Glenn R. Bantug,* Ursula Sauder,‡ Marco Fischer,* Réka Belle,* Leyla Develioglu,* Savaş Tay,† Anja Langenkamp,§ and Christoph Hess*

Effector memory (EM) CD4$^+$ T cells recirculate between normoxic blood and hypoxic tissues to screen for cognate Ag. How mitochondria of these cells, shuttling between normoxia and hypoxia, maintain bioenergetic efficiency and stably uphold antiapoptotic features is unknown. In this study, we found that human EM CD4$^+$ T cells had greater spare respiratory capacity (SRC) than did naive counterparts, which was immediately accessed under hypoxia. Consequently, hypoxic EM cells maintained ATP levels, survived and migrated better than did hypoxic naive cells, and hypoxia did not impair their capacity to produce IFN-γ. EM CD4$^+$ T cells also had more abundant cytosolic GAPDH and increased glycolytic reserve. In contrast to SRC, glycolytic reserve was not tapped under hypoxic conditions, and, under hypoxia, glucose metabolism contributed similarly to ATP production in naive and EM cells. However, both under normoxic and hypoxic conditions, glucose was critical for EM CD4$^+$ T cell survival. Mechanistically, in the absence of glycolysis, mitochondrial membrane potential (ΔΨm) of EM cells declined and intrinsic apoptosis was triggered. Restoring pyruvate levels, the end product of glycolysis, preserved ΔΨm and prevented apoptosis. Furthermore, reconstitution of reactive oxygen species (ROS), whose production depends on ΔΨm, also rescued viability, whereas scavenging mitochondrial ROS exacerbated apoptosis. Rapid access of SRC in hypoxia, linked with built-in, oxygen-resistant glycolytic reserve that functionally insulates ΔΨm and mitochondrial ROS production from oxygen tension changes, provides an immune-metabolic basis supporting survival, migration, and function of EM CD4$^+$ T cells in normoxic and hypoxic conditions. ***The Journal of Immunology*****, 2016, 196: 106–114.**

Upon resolution of an infection, a pool of long-lived memory T cells provides protection from re-exposure to the same pathogen. The pool of circulating memory T cells is heterogeneous. Central memory cells, similar to naive cells, express CCR7 and CD62L and screen lymphoid tissue for reappearance of cognate Ag; in contrast, effector memory (EM) cells express chemokine receptors that guide homing to peripheral tissues, where immune surveillance of potential pathogen re-entry sites occurs (1, 2).

Peripheral tissues, even under homeostatic conditions, are characterized by site-specific low oxygen tension, and O_2 availability is further limited in the context of injury/inflammation, with increased O_2 consumption by infiltrating immune cells, and swelling/edema heightening the distance to the nearest blood vessel (3–7).

Mitochondria are the key ATP-producing site of eukaryotic cells, thus controlling cell life. Interrelated with their capacity to generate ATP, mitochondria also are a central platform orchestrating apoptosis (8). Loss of mitochondrial membrane potential (ΔΨm) plays a dominant role in many scenarios of cell-intrinsic apoptosis. Furthermore, and tightly interlinked with the oxidative phosphorylation (OXPHOS) machinery, mitochondria are a key source of reactive oxygen species (mitochondrial reactive oxygen species [mROS]), which also regulate cell survival (9).

Shuttling between normoxia and hypoxia, mitochondria of EM CD4$^+$ T cells have to maintain ATP fueling of bioenergetically demanding processes, such as migration (10, 11). At the same time, maintaining ΔΨm and tonic mROS production throughout substantial cyclic changes in oxygen availability poses a unique, nonbioenergetic metabolic challenge to EM CD4$^+$ T cells.

Recent work has elucidated how the state of differentiation and activation of T cells impacts on metabolic pathway usage (OXPHOS versus glycolysis) and interrelated effector functionality (12–14). In contrast, the metabolic basis enabling T cell immune surveillance of normoxic and hypoxic tissue sites remains largely unknown. Increased spare respiratory capacity (SRC) has been described as a feature of memory T cells, and augmenting SRC was found to enhance memory CD8$^+$ T cell survival in vivo (15). However, under what circumstances SRC is accessed (e.g., hypoxia, increased work or stress), hence a physiological role of SRC, remains undefined.

*Immunobiology, Department of Biomedicine, University of Basel, 4031 Basel, Switzerland; †Department of Biosystems Science and Engineering, Swiss Federal Institute of Technology in Zurich, 4058 Basel, Switzerland; ‡Microscopy Center, Biocenter, University of Basel, 4056 Basel, Switzerland; and §Roche Pharmaceutical Research and Early Development, Pharmaceutical Sciences, Roche Innovation Center, 4070 Basel, Switzerland

ORCID: 0000-0001-8826-9730 (J.L.).

Received for publication August 5, 2015. Accepted for publication October 26, 2015.

This work was supported by the Roche postdoctoral fellowship program (to S.D.), Swiss National Science Foundation Grants 31003A_135677/1 (to C.H.), 323530-139181 (to M.F.), and PZ00P3_154733/1 (SCORE-Ambizione fellowship to M.M.).

S.D. designed, performed and analyzed most experiments, and wrote the manuscript; M.M. and S.T. designed and performed single-cell migration experiments; C.F., J.L., G.R.B., M.F., R.B., and L.D. performed experiments; U.S. performed transmission electron microscopy; A.L. and C.H. oversaw experiments; and C.H. initiated and oversaw the study, analyzed data, and wrote the manuscript.

Address correspondence and reprint requests to Dr. Sarah Dimeloe and Prof. Christoph Hess, Immunobiology, Department of Biomedicine, University of Basel, 20 Hebelstrasse, CH-4031 Basel, Switzerland. E-mail addresses: sarah.dimeloe@unibas.ch (S.D.) and chess@uhbs.ch (C.H.)

The online version of this article contains supplemental material.

Abbreviations used in this article: 6-AN, 6-aminonicotinamide; DCA, dichloroacetate; 2-DG, 2-deoxyglucose; DMNQ, 2,3-dimethoxy-1,4-naphthoquinone; ECAR, extracellular acidification rate; EM, effector memory; ETC, electron transport chain; HA, heptelidic acid; ΔΨm, mitochondrial membrane potential; mROS, mitochondrial reactive oxygen species; OCR, oxygen consumption rate; OXPHOS, oxidative phosphorylation; PPP, pentose phosphate pathway; ROS, reactive oxygen species; SRC, spare respiratory capacity.

www.jimmunol.org/cgi/doi/10.4049/jimmunol.1501766

Materials and Methods

CD4$^+$ T cell isolation and culture

Blood samples were obtained from healthy donors after written informed consent. The study was approved by the Swiss Red Cross (blood transfusion service) and Institutional Review Board. Bulk CD4$^+$ T cells were isolated as described previously (16) and, unless otherwise indicated, were resuspended in RPMI 1640 containing 10% AB$^+$ human serum, 50 U/ml penicillin, and 50 μg/ml streptomycin (Invitrogen, Carlsbad, CA) (RPMI/10% AB), and 50 IU/ml rIL-2 (PeproTech, Rocky Hill, NJ). Where indicated, positive selection of CD62L$^+$ cells was performed (CD62L microbeads, Miltenyi Biotech, Bergisch Gladbach, Germany) to remove CD62L$^+$ naive and central memory cells from bulk CD4$^+$ T cells, thus enriching EM (CD62L$^-$) cells. Additions to cell culture as indicated included: 2-deoxyglucose (2-DG; Sigma- Aldrich, Schnelldorf, Germany), heptelidic acid (HA; AdipoGen, San Diego, CA), 2,3-dimethoxy-1,4-naphthoquinone (DMNQ; Enzo Life Sciences, Lausen, Switzerland), oligomycin (Sigma-Aldrich), sodium pyruvate (Sigma-Aldrich), MitoTEMPO (Enzo Life Sciences), dichloroacetate (DCA; Sigma-Aldrich), and 6-aminonicotinamide (6-AN; Sigma Aldrich).

Cell lines

Where indicated, Jurkat T cells (obtained from Mike Recher, University of Basel) were cultured in RPMI 1640/10% FCS (Invitrogen), additionally supplemented with GlutaMAX solution (Invitrogen).

Flow cytometry–based cell sorting

For some experiments, flow cytometry–sorted cell populations were used (as indicated). These populations were sorted as naive CD4$^+$ T cells (CD127^{high}CD25^{low}CD45RA$^+$CCR7$^+$) and EM CD4$^+$ T cells (CD127^{high} CD25^{low}CD45RA$^-$CCR7$^-$), and the following mAbs were used: anti-CD45RA mAb–Pacific Blue (clone 2H4; Beckman Coulter, Brea, CA), anti-CD25 mAb–Brilliant Violet 605 (clone 2A3; BD Biosciences, Mountain View CA), anti-CCR7 mAb–PE (clone FABP197; R&D Systems Europe, Abingdon, U.K.), and anti-CD127 mAb–allophycocyanin (clone eBioRDR5; eBioscience, San Diego, CA).

Transmission electron microscopy

Freshly sorted CD4$^+$ T cell subsets were sequentially fixed in 3% paraformaldehyde, 0.5% glutaraldehyde, and 1% osmium tetraoxide, embedded, and then cut into 60-nm sections. Micrographs (×27,000 magnification) were obtained with a Morgagni 268 (FEI, Hillsboro, OR) transmission electron microscope operated at 80 kV. ImageJ software (National Institutes of Health, Bethesda, MD) was used for measuring mitochondrial length (major axis) and width (minor axis). To quantify the morphology of mitochondria from both CD4$^+$ T cell subsets, the average form factor was calculated (major axis to minor axis; an aspect ratio of 1 indicating a circular mitochondrial section).

Confocal microscopy

Confocal microscopy was performed and analyzed as previously described (14). Cells were stained with anti-COX IV (clone 3E11; Cell Signaling Technology, Danvers, MA) or anti-GAPDH (clone D16H11; Cell Signaling Technology), both with secondary goat anti-rabbit 488 (Invitrogen) and DAPI for nuclear staining. All images were processed with ImageJ software (National Institutes of Health).

Flow cytometry

CD4$^+$ T cells were stained with the following mAbs: anti-CD45RA mAb–FITC, –PE, or –allophycocyanin (clone HI100; BD Biosciences) and anti-CCR7 mAb–PE or −allophycocyanin (clone FABP197; R&D Systems Europe). Staining was conducted for 20 min at 4°C followed by two washing steps. Cells were analyzed using the Becton Dickinson FACSCalibur or Accuri flow cytometer.

Assessment of electron transport chain expression

Following surface staining to discriminate cell subsets as described above, cells were fixed/permeabilized for 20 min at room temperature with Cytofix/Cytoperm buffer (BD Biosciences), then washed twice with Perm/Wash buffer (BD Biosciences). Cells were then stained intracellularly with anti-GRIM19 (clone 6E1BH7; Abcam, Cambridge, U.K.), anti-SDHA (clone 2E3GC12FB2AE2; Abcam), anti-UQCRC2 (clone 13G12AF12BB11; Abcam), anti-COXIV (clone 3E11; Cell Signaling Technology), or anti-ATP5A (clone 7H10BD4F9; Abcam) for 30 min at 4°C. Following two further washes with Perm/Wash buffer, cells were stained with secondary goat anti-mouse 488 (Invitrogen, for anti-GRIM19, anti-SDHA, anti-UQCRC2, and anti-ATP5A) or secondary goat anti-rabbit 488 (Invitrogen, for anti-COXIV) for 20 min at 4°C. Control staining with secondary Ab alone was performed in parallel, and the specific fluorescence index was calculated for each subset as: specific Ab fluorescence/secondary Ab fluorescence.

Extracellular metabolic flux analysis

For analysis of the oxygen consumption rate (OCR; in pmol/min) and extracellular acidification rate (ECAR; in mpH/min), the Seahorse XF^{e}96 metabolic extracellular flux analyzer was used (Seahorse Bioscience, North Billerica, MA). Sorted CD4$^+$ T cell subsets were resuspended in serum-free unbuffered RPMI 1640 medium (Sigma-Aldrich) and were plated onto Seahorse cell plates (2.5×10^5 cells per well) coated with Cell-Tak (BD Biosciences) to enhance T cell attachment. Perturbation profiling of the use of metabolic pathways by CD4$^+$ T cells was done by the addition of oligomycin (1 μM), carbonyl cyanide-4-(trifluoromethoxy) phenylhydrazone (2 μM), and rotenone (1 μM; all from Sigma-Aldrich). Metabolic parameters were calculated as described in Supplemental Fig. 1. Additionally, OCR and ECAR were assessed under hypoxic conditions (1% O_2) using the Seahorse XF^{e}96 metabolic extracellular flux analyzer placed in a hypoxia workstation (SCI-tive, Ruskinn Technology, Bridgend, U.K.). Unbuffered medium was equilibrated to hypoxia during 6 h and layered onto sorted CD4$^+$ T cell subsets plated as described above. Metabolic parameters were assessed as per under normoxic conditions and there were additional control wells where 1 M sodium sulfite was injected to calibrant fluid to provide a "zero" oxygen reference parameter for the software algorithm to calculate OCR.

ATP quantification

Sorted CD4$^+$ T cell populations were assessed for total ATP using a bioluminescent ATP assay kit (Abcam). Cells were resuspended at 1×10^6 in RPMI 1640/10% AB and incubated overnight at 37°C in 21% O_2/5% CO_2 or 1% O_2/5% CO_2 as indicated. Then, following baseline luminescence measurements, 10 μl cell suspension was then added to 100 μl reaction mixture containing ATP monitoring enzyme and nucleotide releasing buffer, and luminescence was measured a second time. Each ATP level was calculated as: measurement 2 − measurement 1.

Caspase-9 staining

Caspase-9 staining was performed to identify early, intrinsic apoptotic cells within either sorted CD4$^+$ T cell populations or on bulk CD4$^+$ T cells combined with surface staining to discriminate subpopulations as described above. Staining was performed using caspase-9 FLICA assay as per the manufacturer's instructions (ImmunoChemistry Technologies, Bloomington, MN).

Annexin V staining

Annexin V staining was performed to identify apoptotic cells within either sorted CD4$^+$ T cell populations or on bulk CD4$^+$ T cells combined with surface staining to discriminate subpopulations as described above. Staining was performed using annexin V binding buffer (BD Biosciences) and annexin V conjugated to FITC or allophycocyanin (ImmunoTools, Friesoythe, Germany).

Intracellular cytokine staining

For assessment of IFN-γ production by intracellular cytokine staining, cells were activated for 5 h with PMA (10 ng/ml; Sigma-Aldrich) and ionomycin (500 ng/ml; Sigma-Aldrich). During the final 2 h of activation, cells were treated with monensin solution to block cytokine secretion (BioLegend). Cells were then washed and fixed for 20 min at 37°C (fixation/permeabilization solution, BD Biosciences) and washed with permeabilization buffer (BD Biosciences) prior to staining for 45 min with anti–IFN-γ-PE (clone B27, ImmunoTools), further washing, and analysis.

Transwell migration assays

Isolated CD4$^+$ T cells were resuspended at 5×10^6 cells/ml in RPMI 1640/10% AB and were loaded (100 μl/0.5×10^6 cells) into uncoated 6.5-mm-diameter, 5-μm pore size polycarbonate Transwell inserts (Costar, Corning, NY). One milliliter of RPMI 1640/10% AB R10, or a solution of CXCL12 (10 ng/ml; PeproTech, London, U.K.), was added to the lower well. Where indicated, other compounds were present in both the upper and lower well. Cells were incubated either for 24 h, to assess spontaneous migration, or for 6 h, to assess CXCL12-directed migration at 37°C in 21% O_2/5% CO_2 or 1% O_2/5% CO_2, as indicated. After incubation, cells from

the upper and lower wells were counted with a FACSCalibur and stained for flow cytometry. The migration index indicates the proportion of cells plated in the upper well that migrated to the lower well and was determined by dividing absolute cell counts of migrated cells by absolute cell counts of input cells in the upper well.

Microfluidic migration assays

A full, detailed description of microfluidic migration assays is available in Mehling et al. (17).

$\Delta\Psi m$ measurement

MitoTracker Red staining was performed to assess differences in $\Delta\Psi$m within bulk $CD4^+$ T cells combined with surface staining to discriminate subpopulations. $CD4^+$ T cells (1×10^6/ml) were incubated in RPMI 1640/10% AB with 100 nM MitoTracker Red (Invitrogen) for 20 min at 37˚C/5% CO_2. Cells were then washed twice and stained with mAbs as described above to discriminate cell subsets.

$NADP^+$/NADPH assay

To assess 6-AN inhibitory function, the NADP/NADPH-Glo assay (Promega, Madison, WI) was used according to the manufacturer's instructions with lysate from 1.5×10^6 Jurkat T cells.

Pyruvate dehydrogenase assay

To assess the effect of DCA on pyruvate dehydrogenase activity, a pyruvate dehydrogenase activity colorimetric assay kit (BioVision, Milpitas, CA) was used according to the manufacturer's instructions with lysate from 1×10^6 Jurkat T cells.

Statistical analysis

Data were tested for normality with the Shapiro–Wilkins test. Data with normal distribution were assessed by an unpaired *t* test or, in the case of paired samples, with a paired Student two-sided *t* test. Multiple groups were compared by one- or two-way ANOVA and a Bonferroni posttest for multiple comparisons. Non–normally distributed data were compared using a Mann–Whitney *U* test.

Results

EM $CD4^+$ T cells have more complex mitochondria, express higher levels of electron transport chain protein complexes, and contain more cytosolic GAPDH than do naive cells

First we visualized mitochondria of sorted EM ($CD127^{high}CD25^{low}$ $CD45RA^-CCR7^-$) and naive ($CD127^{high}CD25^{low}CD45RA^+$ $CCR7^+$) $CD4^+$ T cells by transmission electron microscopy. EM $CD4^+$ T cells had more (data not shown) and more complex (elongated/branched) mitochondria than did naive $CD4^+$ T cells (Fig. 1A), and they demonstrated greater MitoTracker staining than did naive cells (16). Consistent with this, COXIV, a subunit of complex IV of the electron transport chain (ETC), was more abundant in EM $CD4^+$ T cells (Fig. 1B), as were all five ETC complexes when assessed by flow cytometry (Fig. 1C). Anaerobic glycolysis can contribute to ATP maintenance when OXPHOS is limited. As a surrogate of the glycolytic machinery, we assessed cytosolic GAPDH expression, which was significantly more abundant in EM cells than in naive counterparts (Fig. 1D). Cytosolic GAPDH has more glycolytic activity than does nuclear GAPDH, and it correlates with glycolytic capacity of human $CD8^+$ T cells (14, 18). Taken together, these ex vivo data established that EM $CD4^+$ T cells, isolated from normoxic blood, had more mitochondria and expressed more cytoplasmic GAPDH than did naive cells.

EM $CD4^+$ T cells have higher OXPHOS and glycolytic capacity than do naive cells

To functionally compare OXPHOS and glycolysis between naive and EM $CD4^+$ T cells, we assessed the OCR and ECAR of sorted naive and EM subsets both under basal conditions and upon mitochondrial perturbation. In normoxic conditions, EM cells had a higher ATP-coupled OCR than did naive cells, as well as greater SRC (Fig. 2A–C, metabolic parameters calculated as described in Supplemental Fig. 1). When tested under hypoxia, ATP-coupled OCR was profoundly reduced in both cell subsets, and interestingly SRC was largely consumed (Fig. 2A–C). Importantly, whereas naive cells almost entirely used their SRC under the conditions tested, EM cells retained residual capacity and demonstrated reduced loss of SRC at hypoxia than did naive cells (Fig. 2C, 2D). Basal ECAR under normoxic conditions was slightly higher in EM $CD4^+$ T cells than in naive cells, consistent with their significantly higher uptake of fluorescently labeled glucose (data not shown). More importantly, EM cells demonstrated glycolytic reserve, which was significantly less in naive cells (Fig. 2E–G). Under hypoxia, basal ECAR increased modestly in both $CD4^+$ T cell subsets, and yet, unexpectedly, glycolytic reserve of EM cells was maintained or even increased (Fig. 2E–G). This remained the case even after exposure to hypoxia for 8 h (data not shown). These data demonstrated that EM $CD4^+$ T cells had higher OXPHOS and glycolytic capacity, and they identified in hypoxic EM cells a dichotomy in usage of OXPHOS versus glycolysis (SRC tapped; glycolytic reserve maintained).

Bioenergetic efficiency and survival of naive and EM $CD4^+$ T cells under normoxic and hypoxic conditions

To directly relate metabolic profiles of naive and EM $CD4^+$ T cells with bioenergetic efficiency, we quantified ATP levels in naive and EM $CD4^+$ T cells cultured in normoxic versus hypoxic conditions. Following 24 h of hypoxia, ATP levels were slightly, but non-significantly, reduced in EM cells, yet they were consistently and significantly reduced in naive cells (Fig. 3A). To discern the contribution of glucose metabolism to ATP maintenance, cells were treated with the glycolysis inhibitor 2-DG (19). This did not markedly impact ATP generation in normoxic naive or EM $CD4^+$ T cells (Fig. 3B), consistent with previous reports (20, 21). Furthermore, also after 4 h of hypoxia there was no significant reduction of the cellular ATP pool in either T cell subset (Fig. 3C, 3D). A significant, yet importantly similar contribution of glucose metabolism to ATP maintenance in naive and EM $CD4^+$ T cells was however observed after 8 and 24 h of hypoxia (Fig. 3B, fold reduction of ATP abundance after 24 h; Fig. 3C, 3D, time course of ATP abundance). These experiments identified a superior capacity of hypoxic EM over naive $CD4^+$ T cells to maintain ATP sufficiency despite comparable contribution of glucose metabolism to the ATP pool, indicating superior oxidative/mitochondrial bioenergetic functionality of EM cells.

We then asked whether increased ATP-coupled respiration and more SRC, as well as the glycolytic reserve of EM $CD4^+$ T cells, imparts a survival benefit under hypoxic conditions. After 24 h, a marked increase in caspase-9 activity, an early indication of intrinsic, that is, mitochondria-triggered, apoptosis (8), was observed in hypoxic naive, but not in hypoxic EM, $CD4^+$ T cells (Fig. 4A, 4B). In the naive subpopulation, annexin V staining, a marker of late apoptosis, was also modestly but consistently increased at this time point (Fig. 4C). When cultures were extended to 72 h, increased annexin V staining was detected in both hypoxic naive and EM $CD4^+$ T cells, yet less so in the EM subset (Fig. 4D, 4E). To discern the importance of glucose metabolism to the survival of normoxic and hypoxic naive and EM $CD4^+$ T cells, 2-DG was added to the cell cultures (24 h). The proportion of naive cells with detectable caspase-9 activity was unchanged in normoxic conditions when cultured with 2-DG (Fig. 4F). Under hypoxic conditions, naive cells, already coping badly with hypoxia as evidenced by their much higher proportion of caspase-9 positivity as compared with EM cells, depended on glucose for

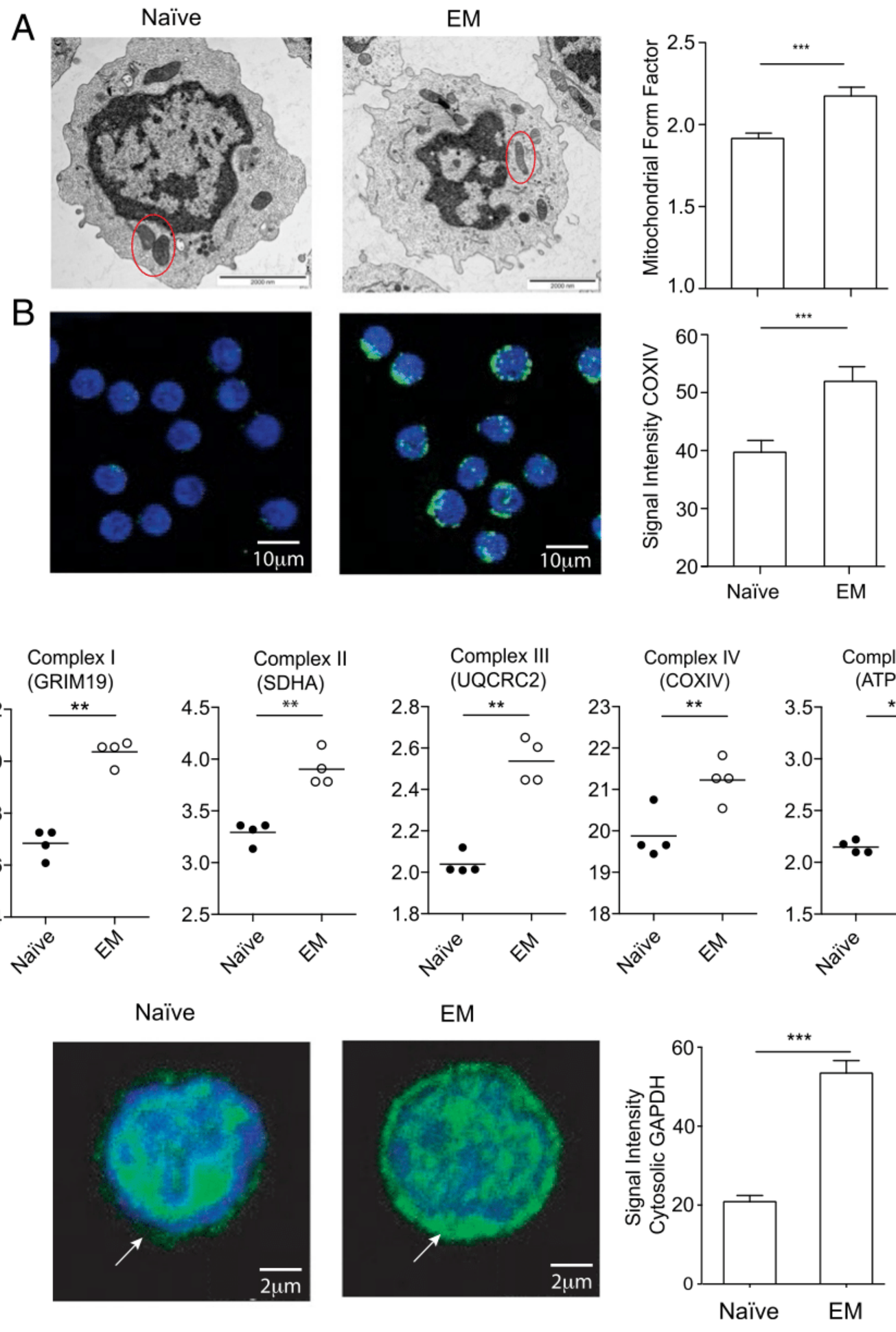

FIGURE 1. EM CD4$^+$ T cells have more, and more complex mitochondria, increased electron transport chain expression, and greater cytosolic GAPDH than do naive cells. (**A**) Representative electron microscopy images (fixed and stained with osmium tetroxide) of sorted naive and EM CD4$^+$ T cells (*left*), and quantification (*right*) of mitochondrial form factor (length/width) (n = 337 naive and 366 EM cells from three individual donors analyzed; mitochondria are circled in red). Scale bars, 2000 nm (*left* and *middle*). (**B**) Abundance of COXIV in naive and EM CD4$^+$ T cells assessed by confocal microscopy (*left*) (DAPI- and Alexa Fluor–stained) and quantification of COXIV-specific signal intensity (*right*) (n = 234 naive and 240 EM cells from three individual donors analyzed). (**C**) ETC expression assessed by intracellular staining and flow cytometry of individual complexes, and expressed as mean specific fluorescence index (SFI) relative to control secondary Ab staining (n = 4 individual donors). (**D**) Representative confocal microscopy images (*left*) and quantification of cytosolic GAPDH specific signal intensity (*right*) among naive and EM CD4$^+$ T cells (n = 62 naive and 103 EM cells from three individual donors analyzed) (DAPI- and Alexa Fluor–stained). The p values were calculated by a paired t test. *$p < 0.05$, **$p < 0.01$, ***$p < 0.001$.

survival (Fig. 4F). However, blocking glucose metabolism for only 24 h in both normoxic and hypoxic EM cells increased the proportion of both early and late apoptotic cells, that is, caspase-9$^+$ and annexin V$^+$ cells, respectively (Fig. 4F, FG), indicating a key role for glucose metabolism in EM cell survival, regardless of oxygen availability.

A critical function of EM CD4$^+$ T cells is the rapid production of cytokines, such as the signature memory cytokine IFN-γ, upon Ag re-encounter. We hypothesized that exposure to hypoxia should not adversely impact a subsequent memory response, because EM CD4$^+$ T cells, unlike naive cells, survive well under these conditions. Conversely, limitation of glucose metabolism, which selectively induced apoptosis of memory cells, should diminish cytokine responses. To directly assess this, CD4$^+$CD62L$^-$-enriched T cells were activated following a period of culture at normoxia or hypoxia (both with 10 mM glucose), or with 0 mM glucose for 24 h. Glucose deprivation, rather than 2-DG, was employed to avoid unwanted inhibition of glycolysis during subsequent activation. Cells were then activated with PMA and ionomycin to assess the cytokine response. Activation took place under normoxia and in presence of 10 mM glucose. Indeed, hypoxia had no significant effect on the frequency of IFN-γ$^+$ cells, whereas glucose deprivation significantly reduced numbers of cytokine-producing cells (Fig. 4H–J).

EM CD4$^+$ T cells better maintain motility under ATP-limiting conditions

Next we tested how metabolic profiles of CD4$^+$ T cells related to their migration, which is highly ATP-dependent and fundamental to immune surveillance of peripheral tissues (10, 11). At bulk and single-cell levels (using a Transwell assay and microfluidic system, respectively), we first defined spontaneous and chemokine (CXCL12)-directed migratory properties of CD4$^+$ T cell populations. These assays established a clear difference in spontaneous as well as chemokine-directed migration of CD4$^+$ T cell subsets, with increased migration of EM cells (Supplemental Fig. 2). Under low oxygen concentrations, or when mimicking hypoxia with 0.4 μM oligomycin (11), EM CD4$^+$ T cells were significantly better able to maintain spontaneous and CXCL12-directed migration than were naive cells, in both the Transwell system (Fig. 5A, *upper panels*, 5B) and when assessing migration of single cells (Fig. 5C, 5D). Blockade of glycolysis with 2-DG did not impair CXCL12-directed migration of either naive or EM CD4$^+$ T cells in the Transwell assay under normoxic or hypoxic

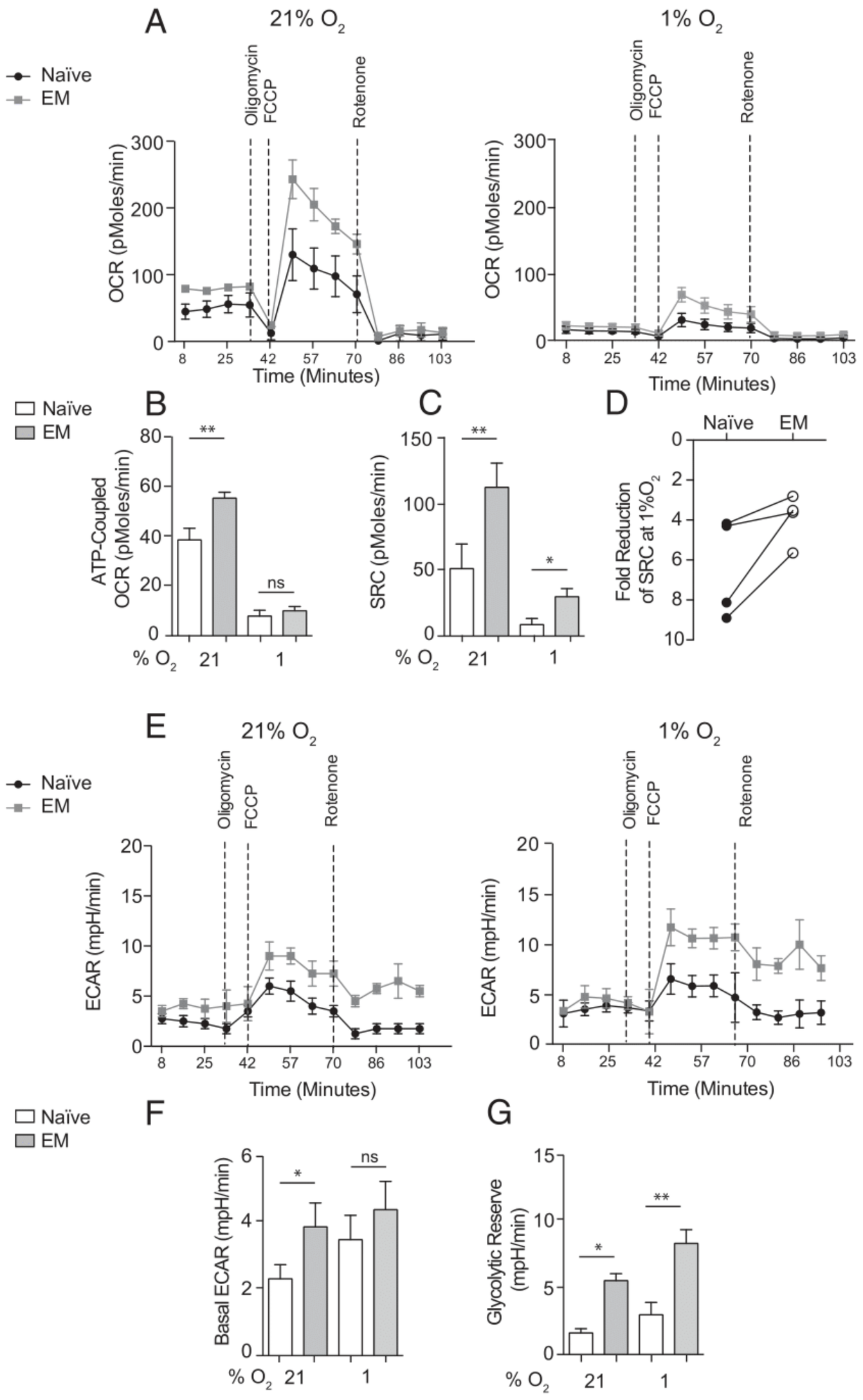

FIGURE 2. Oxidative and glycolytic metabolism of naive and EM $CD4^+$ T cells under normoxic and hypoxic conditions. (**A**) Mean OCR of sorted naive (black line) and EM (gray line) $CD4^+$ T cells, measured before and after addition of oligomycin, carbonyl cyanide-4-(trifluoromethoxy)phenylhydrazone (FCCP), and rotenone at 21% O_2 ($n = 8$ individual donors) (*left panel*) and 1% O_2 ($n = 4$ individual donors) (*right panel*). (**B** and **C**) Mean ATP-coupled OCR (B) and SRC (C) of naive and EM cells at 21% O_2 ($n = 8$ individual donors) and 1% O_2 ($n = 4$ individual donors). (**D**) Fold reduction of SRC among naive and EM $CD4^+$ T cells at 1% O_2 compared with 21% O_2 ($n = 4$ individual donors). (**E**) Mean ECAR of naive and EM $CD4^+$ T cells treated as described in (A) at 21% O_2 ($n = 8$ individual donors) (*left panel*) and 1% O_2 ($n = 4$ individual donors) (*right panel*). (**F** and **G**) Mean basal ECAR (F) and glycolytic reserve (G) of naive and EM cells at 21% ($n = 8$ individual donors) and 1% O_2 ($n = 4$ individual donors). The p values were calculated by a paired t test (D) or one-way ANOVA and a Bonferroni posttest. $*p < 0.05$, $**p < 0.01$, $***p < 0.001$.

conditions (Fig. 5B, *lower panel*). This is consistent with the data in Fig. 3, which show that 2-DG treatment did not deplete ATP under normoxia, or until after 8 h of exposure to hypoxia. However, effects of limited glucose metabolism on migration beyond 6–8 h were not tested in this assay. Taken together with the data in Fig. 3, these observations indicated that mitochondrial bioenergetics, reflected in increased SRC and ATP-coupled respiration, and, importantly, residual SRC even under hypoxia, constituted a critical determinant of EM $CD4^+$ T cell migration under hypoxic conditions by ensuring ATP sufficiency.

Glycolysis-derived pyruvate regulates survival of EM $CD4^+$ T cells via maintenance of $\Delta\Psi$m and mROS production

We reasoned that both the bioenergetic advantage, as well as the oxygen-insensitive glucose-dependent survival mechanism of EM $CD4^+$ T cells, might reflect an interrelated adaptation of these cells enabling their periodic migration into hypoxic tissues. Furthermore, we considered that functionally "insulating" $\Delta\Psi$m and/or mROS production from oxygen availability may be advantageous. Thus, we hypothesized that, by providing pyruvate to fuel the tricarboxylic acid cycle, glucose metabolism stabilizes $\Delta\Psi$m and downstream mROS production. To test this hypothesis, we investigated the interrelation of glycolysis, $\Delta\Psi$m, mROS production, and T cell survival.

First, we confirmed that removal of glucose for 24 h induced apoptosis of normoxic and hypoxic EM cells similarly to pharmacologically blocking glycolysis with 2-DG (Fig. 6A). This approach additionally allowed us to observe that apoptosis was prevented in the presence of very low-level glucose (0.5 mM), making it unlikely that in vivo glucose availability readily becomes a limiting factor of this survival-regulating axis (Fig. 6A). Next, to narrow down the glycolytic intermediate mediating the antiapoptotic effect in EM $CD4^+$ T cells, we inhibited glycolysis at the level of GAPDH (using HA or iodoacetate) to compare with 2-DG,

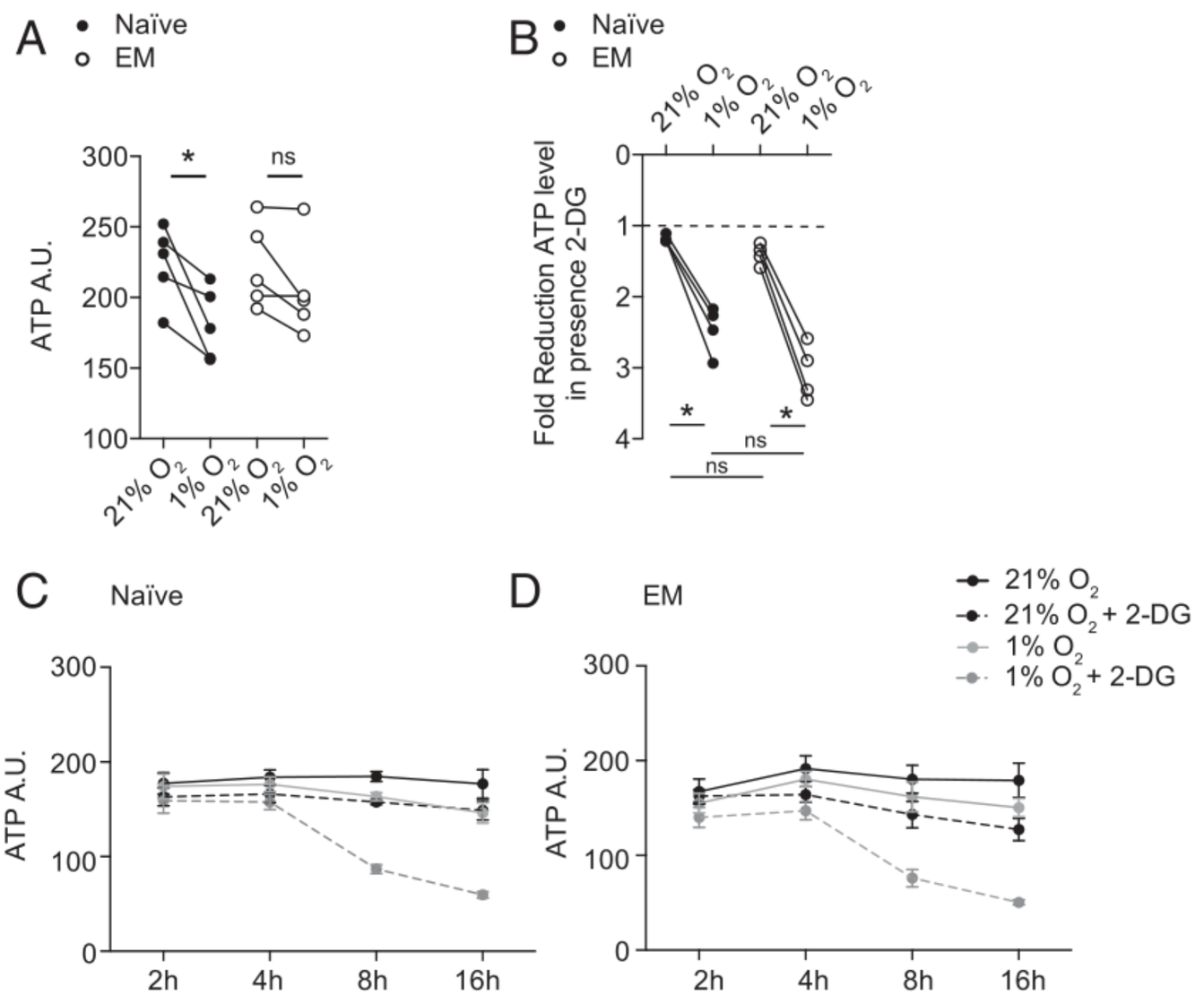

FIGURE 3. ATP content of naive and EM $CD4^+$ T cells under normoxic and hypoxic conditions: contribution of OXPHOS and glycolysis. (**A**) ATP abundance (arbitrary units [A.U.]) in naive and EM $CD4^+$ T cells, measured after 24 h of culture at either 21% or 1% O_2 ($n = 5$ individual donors). (**B**) Fold reduction and (**C** and **D**) raw data (arbitrary units) of ATP levels among naive and EM $CD4^+$ T cells cultured in the presence of 10 mM 2-DG for (B) 16 h and (C and D) times indicated at either 21 or 1% O_2 ($n = 7$ individual donors). The p values were calculated by one-way ANOVA and a Bonferroni posttest. $^*p < 0.05$.

which is phosphorylated by hexokinase and subsequently inhibits downstream glycolytic enzymes, thus blocking additionally the pentose phosphate pathway (PPP) (19). Apoptosis was also significantly induced in EM $CD4^+$ T cells by GAPDH inhibition (Supplemental Fig. 3A, 3B). In oocytes, PPP-derived NADPH has been demonstrated to be important for cell survival via generation of NADPH, which in turn activates CaMK-II to phosphorylate and inhibit caspase-2 (22). The finding that HA and iodoacetate, which inhibit glycolysis after the branch-off of the PPP, also significantly induced apoptosis argued against a major role of this pathway in regulating EM $CD4^+$ T cell survival. To directly probe for a role of the PPP in regulating $CD4^+$ T cell apoptosis, we blocked entry of glucose-6-phosphate into the PPP by inhibiting glucose-6-phosphate dehydrogenase with 6-AN, which, as expected, effectively reduced cellular NADPH levels (Supplemental Fig. 3C, 3D). No increased rates of apoptosis were observed in these experiments

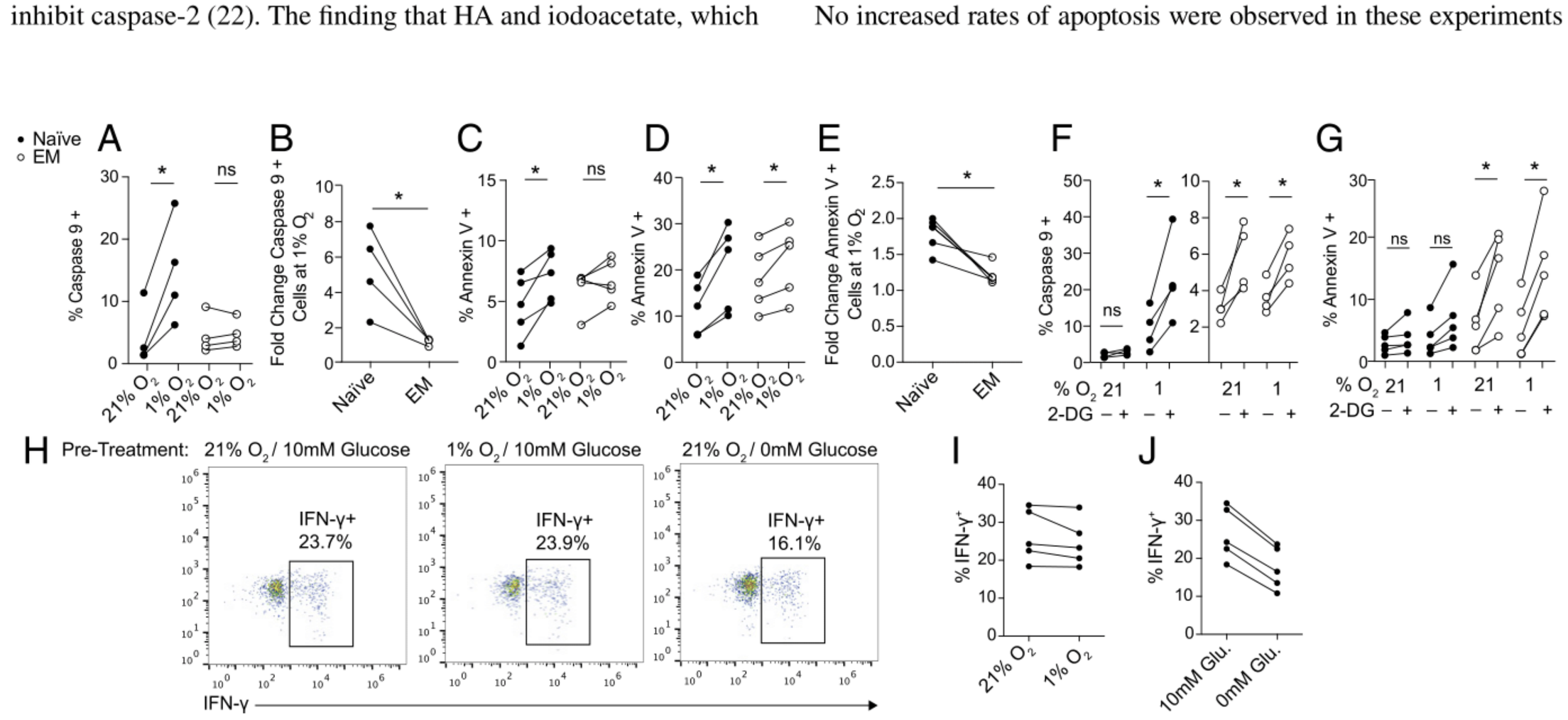

FIGURE 4. Survival and function of naive and EM $CD4^+$ T cells under normoxic and hypoxic conditions: contribution of OXPHOS and glycolysis. (**A** and **B**) Flow cytometry–based assessment of caspase-9 activity among naive and EM $CD4^+$ T cells after 24 h of normoxia versus hypoxia, indicated as percentage positive (+) cells (A) and fold change at 1% as compared with 21% O_2 (B) ($n = 4$ individual donors). (**C**–**E**) Flow cytometry–based assessment of annexin V positivity (+) among naive and EM $CD4^+$ T cells after (C) 24 h and (D) 72 h of normoxia versus hypoxia, indicated as percentage positive (+) cells, and (E) fold change at 1% as compared with 21% O_2 at 72 h [(C)–(E); $n = 5$ individual donors]. (**F**) Flow cytometry–based assessment of caspase-9 activity (+) among naive and EM $CD4^+$ T cells after 24 h of normoxia versus hypoxia, and in presence or absence of 10 mM 2-DG. (**G**) Flow cytometry–based assessment of annexin V positivity (+) among naive and EM $CD4^+$ T cells after 24 h of normoxia versus hypoxia, and in presence or absence of 10 mM 2-DG [(F) and (G); $n = 4$ individual donors]. (**H**) Representative example of the frequency IFN-γ–producing cells among $CD4^+CD62L^-$ T cells cultured for 24 h in normal RPMI 1640/10% AB containing 10 mM glucose, either at 21% O_2 or 1% O_2, or in glucose-free medium/10% dialyzed glucose-free serum (0 mM glucose) and subsequently activated with PMA/ionomycin for 5 h under control conditions. (**I** and **J**) Summary of frequencies of IFN-γ^+ cells following culture as in (H) ($n = 5$ individual donors). The p values were calculated by one-way ANOVA and a Bonferroni posttest (A, C, E, G, and H) or paired t test (B, D, F, I, and J). $^*p < 0.05$, $^{**}p < 0.01$, $^{***}p < 0.001$.

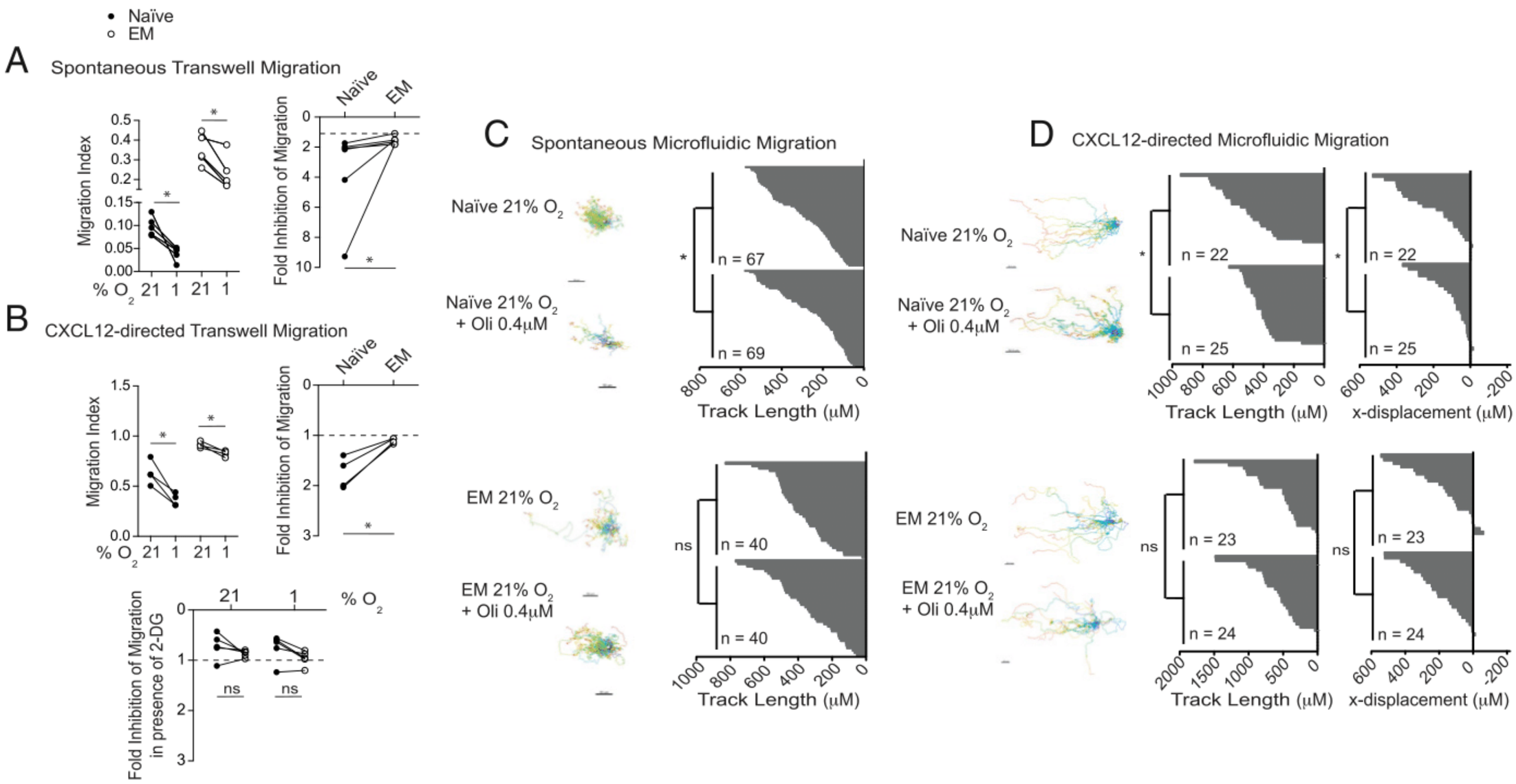

FIGURE 5. EM CD4$^+$ T cells maintain a high level of motility under hypoxia or hypoxia-mimicking conditions. (**A** and **B**) Migration efficiency of naive and EM CD4$^+$ T cells in Transwell migration assays was compared between normoxic conditions and hypoxic conditions and with/without 10 mM 2-DG. Data are expressed as migration indices and "fold inhibition of migration" by relating to migration at 21% O_2 or in absence of 2-DG. (A) Naive and EM subsets migrating spontaneously (24 h) (n = 6 individual donors). (B) Naive and EM subsets migrating in a gradient of CXCL12 (6 h) (n = 4 individual donors). (**C** and **D**) Spontaneous and chemokine-directed migration of naive versus EM CD4$^+$ T cells was directly monitored at a single-cell level after placing cells in fibronectin-coated microfluidic devices (17). The position of each cell was recorded every minute, and trajectories of migrating cells were analyzed. These experiments, performed at 21% O_2 and under hypoxia-mimicking conditions (oligomycin 0.4 μM) (11), indicated that also at a single-cell level EM cells better retained their migratory capacity than did naive counterparts, both when moving spontaneously [(C), *upper panels* versus *lower panels*], as well as in stable, diffusion-based chemotactic gradients of CXCL12 [(D), *upper panels* versus *lower panels*]. The p values were calculated by a paired t test. *$p < 0.05$, **$p < 0.01$.

(Supplemental Fig. 3E). Furthermore, NADPH was largely undetectable in these quiescent CD4$^+$ T cells (data not shown). In all, a prominent role of the PPP in regulating apoptosis of EM CD4$^+$ T cells thus could be excluded. In contrast, adding pyruvate (the end product of glycolysis) to 2-DG–treated CD4$^+$ T cells significantly reduced apoptosis (Fig. 6B), as did treatment with DCA (Supplemental Fig. 3F), which inhibits pyruvate dehydrogenase kinase, thereby promoting activity of pyruvate dehydrogenase (Supplemental Fig. 3G), and hence conversion of residual pyruvate into mitochondrial acetyl-CoA. These observations are in line with a recent report that described exogenous sodium pyruvate to rescue glucose-deprived bulk murine T cells from apoptosis (23). Supporting the idea that pyruvate was important in maintaining $\Delta\Psi$m to prevent intrinsic apoptosis, 2-DG reduced $\Delta\Psi$m in EM CD4$^+$ T cells (Fig. 6C), and adding back pyruvate significantly increased $\Delta\Psi$m (Fig. 6D). Furthermore, dissipation of $\Delta\Psi$m by oligomycin treatment abrogated the protective effect of pyruvate (Fig. 6E). Consistent with the data shown in Fig. 4F, oligomycin alone, similar to hypoxia, caused apoptosis in naive cells, but not EM cells, which was exacerbated by blockade of glycolysis (Fig. 6E). Maintenance of $\Delta\Psi$m not only prevents cell-intrinsic apoptosis pathways (8, 9), but it also is critical for the generation of mROS (9–11). Because sodium pyruvate has intrinsic antioxidant capacity (24), it was not possible to reliably assess its effect on cellular or mROS levels. However, to discern whether ROS constituted a survival signal selectively for EM CD4$^+$ T cells, we either scavenged mROS with the mitochondrial-targeted antioxidant MitoTEMPO or augmented cellular ROS generation using DMNQ, a redox-cycling agent that induces intracellular superoxide anion formation. mROS scavenging promoted 2-DG–induced apoptosis of EM CD4$^+$ T cells, but it did not affect naive cells (Fig. 6F). Conversely, augmenting ROS levels, similar to pyruvate, completely abrogated apoptosis induced by inhibiting glycolysis (Fig. 6G).

Discussion

Metabolic adaptation to acute and chronic hypoxia has been studied extensively in various biologic systems. However, adaptation of EM CD4$^+$ T cells, which are by default cycling between normoxic blood and hypoxic nonlymphoid tissues, poses a metabolic challenge that has not yet been explored.

In this study, we observed that key metabolic features of human EM CD4$^+$ T cells were 1) their increased mitochondrial content, reflected in higher SRC and ATP-coupled respiration, and 2) more abundant cytosolic GAPDH and glycolytic reserve. SRC was linked with bioenergetic fitness and enabled hypoxic EM cells to better maintain ATP levels, survive, and migrate under hypoxic conditions than naive counterparts. EM CD4$^+$ T cell survival under hypoxia also ensured unhampered cytokine recall responses. These findings are consistent with observations that memory CD8$^+$ T cells overexpressing the mitochondrial fatty acid transporter carnitine palmitoyltransferase, which affords them greater SRC, survive better in vivo than do control cells (15). However, until now it has been unclear in what context cells rely on their SRC—under stress, increased workload, or limited resources. In this study, to our knowledge for the first time, we were able to demonstrate that under hypoxia SRC is immediately accessed, but importantly in naive CD4$^+$ T cells is virtually exhausted, whereas the greater SRC of EM cells ensures, even under hypoxia, respiratory reserve.

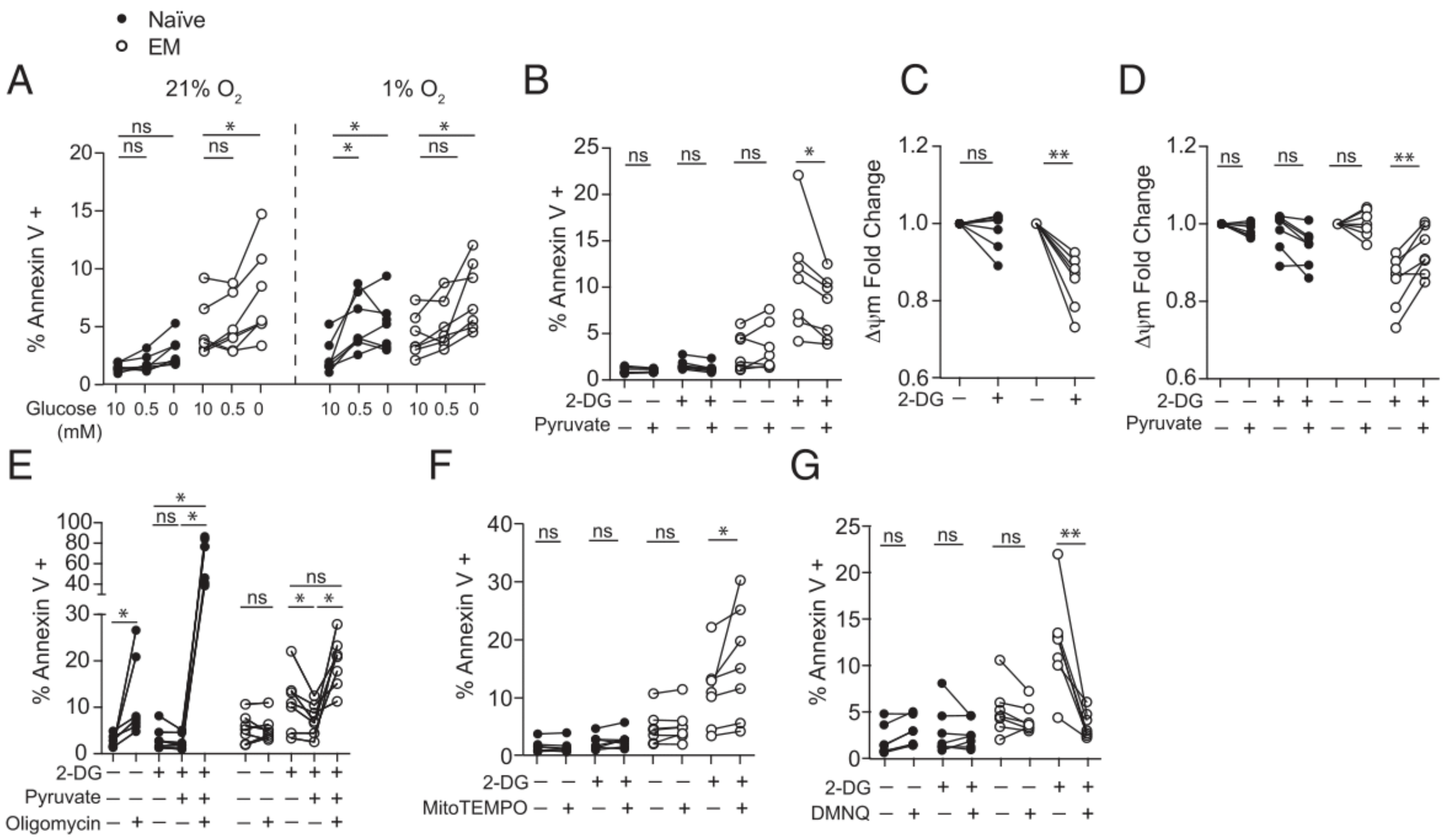

FIGURE 6. Glycolysis regulates EM CD4$^+$ T cell survival via maintenance of $\Delta\psi$m and ROS generation. (**A**) Percentage of annexin V$^+$ naive and EM CD4$^+$ T cells cultured for 24 h in normal RPMI 1640/10% AB containing 10 mM glucose, glucose-free medium/10% dialyzed glucose-free serum, or glucose-free medium/10% dialyzed glucose-free serum reconstituted with 0.5 mM glucose, each under normoxic versus hypoxic conditions. (**B**) Percentage of annexin V$^+$ naive and EM CD4$^+$ T cells cultured for 24 h in normal RPMI 1640/10% AB containing 10 mM glucose, with/without 10 mM pyruvate, and with/without 10 mM 2-DG. (**C** and **D**) Change of $\Delta\Psi$m among naive and EM CD4$^+$ T cells cultured for 24 h in normal RPMI 1640/10% AB containing 10 mM glucose with/without 10 mM 2-DG (C) and/or 10mM pyruvate (D) relative to cells cultured for 24 h in medium alone. (**E**) Percentage of Annexin V$^+$ naive and EM CD4$^+$ T cells cultured for 24 h in normal RPMI 1640/10% AB containing 10 mM glucose with/without 10 mM 2-DG, with/without 10 mM pyruvate, 10 mM glucose with/without 10 mM 2-DG, with/without 1 μM oligomycin. (**F**) Percentage of annexin V$^+$ naive and EM CD4$^+$ T cells cultured for 24 h in normal RPMI 1640/10% AB containing 10 mM glucose with/without 10 mM 2-DG, with/without 50 μM MitoTEMPO. (**G**) Percentage of annexin V$^+$ naive and EM CD4$^+$ T cells cultured for 24 h in normal RPMI 1640/10% AB containing 10 mM glucose with/without 10 mM 2-DG, with/without 10 mM DMNQ. (A)–(G), $n = 7$ individual donors. The p values were calculated by two-way ANOVA and a Bonferroni posttest. *$p < 0.05$, **$p < 0.01$.

Glucose metabolism did not markedly contribute to ATP maintenance in naive or EM CD4$^+$ T cells under normoxia. This is consistent with previous reports (20, 21) and consistent with the fact that T cells have the capacity to use both fatty acid oxidation and glutaminolysis to provide tricarboxylic acid cycle substrates and thereby maintain cellular bioenergetics (12, 21). After 4–8 h of hypoxia, glucose metabolism did significantly contribute to ATP sufficiency—intriguingly, however, to a similar extent in both naive and EM CD4$^+$ T cells despite the increased glycolytic reserve of EM CD4$^+$ T cells. Indeed, contrary to SRC, glycolytic reserve was not tapped by hypoxic EM CD4$^+$ T cells, even after several hours of exposure to hypoxia. In murine models, Notch signaling in CD4$^+$ T cells was recently found to regulate glucose uptake, which was suggested to enable memory cells to constantly acquire energy for their maintenance (23). We found that glycolysis, which was functional in the presence of as little as 0.5 mM glucose, surprisingly fulfilled an important nonbioenergetic role. Selectively in EM CD4$^+$ T cells, glycolysis, via pyruvate, maintained $\Delta\Psi$m, which was key to regulating their survival and capacity to mount cytokine responses upon activation. We propose that glycolysis-driven stabilization of $\Delta\Psi$m functionally insulates important survival signals from large differences in oxygen concentration experienced by EM cells as they circulate into, and out of, peripheral tissues.

Recent work has elucidated that T cells undergo significant changes in metabolism during TCR- and costimulation-driven clonal expansion and differentiation, which critically support these processes (12). In the present study, in contrast, we assessed metabolic features of steady-state, nonactivated cells in relationship to their survival and function under normoxic and hypoxic conditions. It is interesting that glycolysis not only plays an important nonbioenergetic role during immune recall (14, 25), but it also is critically required in the context of immune surveillance. Increased glycolytic capacity has recently been proposed as a hallmark of immune-experienced cells ("trained immunity") (26). Mechanistically linking nonbioenergetic aspects of glycolysis to EM CD4$^+$ T cell survival adds an important facet to this concept.

A scaled-up OXPHOS machinery endows EM CD4$^+$ T cells with a bioenergetic advantage, which, however, comes at the cost of having to maintain the $\Delta\Psi$m of an increased mitochondrial mass to prevent intrinsic apoptosis. It is thus plausible that a $\Delta\Psi$m stabilizing axis, as described in this study, coevolves with mitochondrial biogenesis. Other examples of $\Delta\Psi$m stabilizing mechanisms include the calcium-binding mitochondrial carrier protein SCaMC-1 (SLC25A24), which buffers intramitochondrial calcium to prevent membrane depolarization (27), and recruitment of hexokinase II to the outer mitochondrial membrane. Mitochondrial localization of hexokinase II is proposed to stabilize $\Delta\Psi$m via physical interaction with mitochondrial membrane proteins, or by maintaining local ADP levels or increasing glucose-mediated OXPHOS (28).

ROS, long known to cause oxidative damage to cellular membranes, proteins, and DNA, have recently been assigned important roles as signaling intermediates in T cells. During T cell activation, ROS derived from mitochondrial complex III critically underpin IL-2 production and proliferation (29). Furthermore, activated T cells from individuals with rheumatoid arthritis demonstrate reduced abundance of ROS, associated with increased apoptosis, which could be recapitulated in healthy cells by scavenging mROS (30). ROS thus constitute both a survival and differentiation signal

for T cells, as also described for stem cells (9). Of note, EM CD4$^+$ T cells possess more cell-intrinsic antioxidant mechanisms, and are characterized by lower steady-state ROS levels than are naive cells (31). This may protect these cells from high levels of exogenous ROS encountered in inflamed environments. Our data suggest that a decline in $\Delta\Psi$m, which determines mROS production (8, 9), dropped mROS levels below the minimum required for their survival, making the cells critically dependent on $\Delta\Psi$m-stabilizing glycolysis.

In summary, our findings identify that SRC is immediately accessed by hypoxic EM CD4$^+$ T cells to maintain bioenergetic sufficiency, and assign to glycolysis a nonbioenergetic role: largely uncoupled from oxygen concentration, glycolysis provides pyruvate to stabilize $\Delta\Psi$m, thus functionally insulating mitochondria of EM CD4$^+$ T cells from cycling changes in oxygen concentrations.

Acknowledgments

We thank E. Traunecker and T. Krebs for technical support with cell sorting, and A. Buser (University Hospital Basel) for buffy coats.

Disclosures

The authors have no financial conflicts of interest.

References

1. Sallusto, F., D. Lenig, R. Förster, M. Lipp, and A. Lanzavecchia. 1999. Two subsets of memory T lymphocytes with distinct homing potentials and effector functions. *Nature* 401: 708–712.
2. Mueller, S. N., T. Gebhardt, F. R. Carbone, and W. R. Heath. 2013. Memory T cell subsets, migration patterns, and tissue residence. *Annu. Rev. Immunol.* 31: 137–161.
3. Spence, V. A., and W. F. Walker. 1984. Tissue oxygen tension in normal and ischaemic human skin. *Cardiovasc. Res.* 18: 140–144.
4. Braun, R. D., J. L. Lanzen, S. A. Snyder, and M. W. Dewhirst. 2001. Comparison of tumor and normal tissue oxygen tension measurements using OxyLite or microelectrodes in rodents. *Am. J. Physiol. Heart Circ. Physiol.* 280: H2533–H2544.
5. Caldwell, C. C., H. Kojima, D. Lukashev, J. Armstrong, M. Farber, S. G. Apasov, and M. V. Sitkovsky. 2001. Differential effects of physiologically relevant hypoxic conditions on T lymphocyte development and effector functions. *J. Immunol.* 167: 6140–6149.
6. Karhausen, J., G. T. Furuta, J. E. Tomaszewski, R. S. Johnson, S. P. Colgan, and V. H. Haase. 2004. Epithelial hypoxia-inducible factor-1 is protective in murine experimental colitis. *J. Clin. Invest.* 114: 1098–1106.
7. Campbell, E. L., W. J. Bruyninckx, C. J. Kelly, L. E. Glover, E. N. McNamee, B. E. Bowers, A. J. Bayless, M. Scully, B. J. Saeedi, L. Golden-Mason, et al. 2014. Transmigrating neutrophils shape the mucosal microenvironment through localized oxygen depletion to influence resolution of inflammation. *Immunity* 40: 66–77.
8. Green, D. R., L. Galluzzi, and G. Kroemer. 2014. Cell biology. Metabolic control of cell death. *Science* 345: 1250256.
9. Chandel, N. S. 2014. Mitochondria as signaling organelles. *BMC Biol.* 12: 34.
10. Gebhardt, T., P. G. Whitney, A. Zaid, L. K. Mackay, A. G. Brooks, W. R. Heath, F. R. Carbone, and S. N. Mueller. 2011. Different patterns of peripheral migration by memory CD4$^+$ and CD8$^+$ T cells. *Nature* 477: 216–219.
11. Campello, S., R. A. Lacalle, M. Bettella, S. Mañes, L. Scorrano, and A. Viola. 2006. Orchestration of lymphocyte chemotaxis by mitochondrial dynamics. *J. Exp. Med.* 203: 2879–2886.
12. Pearce, E. L., M. C. Poffenberger, C.-H. Chang, and R. G. Jones. 2013. Fueling immunity: insights into metabolism and lymphocyte function. *Science* 342: 1242454.
13. van der Windt, G. J., D. O'Sullivan, B. Everts, S. C. Huang, M. D. Buck, J. D. Curtis, C.-H. Chang, A. M. Smith, T. Ai, B. Faubert, et al. 2013. CD8 memory T cells have a bioenergetic advantage that underlies their rapid recall ability. *Proc. Natl. Acad. Sci. USA* 110: 14336–14341.
14. Gubser, P. M., G. R. Bantug, L. Razik, M. Fischer, S. Dimeloe, G. Hoenger, B. Durovic, A. Jauch, and C. Hess. 2013. Rapid effector function of memory CD8$^+$ T cells requires an immediate-early glycolytic switch. *Nat. Immunol.* 14: 1064–1072.
15. Pearce, E. L., M. C. Walsh, P. J. Cejas, G. M. Harms, H. Shen, L.-S. Wang, R. G. Jones, and Y. Choi. 2009. Enhancing CD8 T-cell memory by modulating fatty acid metabolism. *Nature* 460: 103–107.
16. Dimeloe, S., C. Frick, M. Fischer, P. M. Gubser, L. Razik, G. R. Bantug, M. Ravon, A. Langenkamp, and C. Hess. 2014. Human regulatory T cells lack the cyclophosphamide-extruding transporter ABCB1 and are more susceptible to cyclophosphamide-induced apoptosis. *Eur. J. Immunol.* 44: 3614–3620.
17. Mehling, M., T. Frank, C. Albayrak, and S. Tay. 2015. Real-time tracking, retrieval and gene expression analysis of migrating human T cells. *Lab Chip* 15: 1276–1283.
18. Mazzola, J. L., and M. A. Sirover. 2003. Subcellular localization of human glyceraldehyde-3-phosphate dehydrogenase is independent of its glycolytic function. *Biochim. Biophys. Acta* 1622: 50–56.
19. Barban, S., and H. O. Schultze. 1961. The effects of 2-deoxyglucose on the growth and metabolism of cultured human cells. *J. Biol. Chem.* 236: 1887–1890.
20. Tripmacher, R., T. Gaber, R. Dziurla, T. Häupl, K. Erekul, A. Grützkau, M. Tschirschmann, A. Scheffold, A. Radbruch, G.-R. Burmester, and F. Buttgereit. 2008. Human CD4$^+$ T cells maintain specific functions even under conditions of extremely restricted ATP production. *Eur. J. Immunol.* 38: 1631–1642.
21. Blagih, J., F. Coulombe, E. E. Vincent, F. Dupuy, G. Galicia-Vázquez, E. Yurchenko, T. C. Raissi, G. J. W. van der Windt, B. Viollet, E. L. Pearce, et al. 2015. The energy sensor AMPK regulates T cell metabolic adaptation and effector responses in vivo. *Immunity* 42: 41–54.
22. Nutt, L. K., S. S. Margolis, M. Jensen, C. E. Herman, W. G. Dunphy, J. C. Rathmell, and S. Kornbluth. 2005. Metabolic regulation of oocyte cell death through the CaMKII-mediated phosphorylation of caspase-2. *Cell* 123: 89–103.
23. Maekawa, Y., C. Ishifune, S. Tsukumo, K. Hozumi, H. Yagita, and K. Yasutomo. 2015. Notch controls the survival of memory CD4$^+$ T cells by regulating glucose uptake. *Nat. Med.* 21: 55–61.
24. Shostak, A., L. Gotloib, R. Kushnier, and V. Wajsbrot. 2000. Protective effect of pyruvate upon cultured mesothelial cells exposed to 2 mM hydrogen peroxide. *Nephron* 84: 362–366.
25. Chang, C.-H., J. D. Curtis, L. B. Maggi, Jr., B. Faubert, A. V. Villarino, D. O'Sullivan, S. C.-C. Huang, G. J. W. van der Windt, J. Blagih, J. Qiu, et al. 2013. Posttranscriptional control of T cell effector function by aerobic glycolysis. *Cell* 153: 1239–1251.
26. Cheng, S.-C., J. Quintin, R. A. Cramer, K. M. Shepardson, S. Saeed, V. Kumar, E. J. Giamarellos-Bourboulis, J. H. A. Martens, N. A. Rao, A. Aghajanirefah, et al. 2014. mTOR- and HIF-1α-mediated aerobic glycolysis as metabolic basis for trained immunity. *Science* 345: 1250684.
27. Traba, J., A. Del Arco, M. R. Duchen, G. Szabadkai, and J. Satrústegui. 2012. SCaMC-1 promotes cancer cell survival by desensitizing mitochondrial permeability transition via ATP/ADP-mediated matrix Ca^{2+} buffering. *Cell Death Differ.* 19: 650–660.
28. Nederlof, R., O. Eerbeek, M. W. Hollmann, R. Southworth, and C. J. Zuurbier. 2014. Targeting hexokinase II to mitochondria to modulate energy metabolism and reduce ischaemia-reperfusion injury in heart. *Br. J. Pharmacol.* 171: 2067–2079.
29. Sena, L. A., S. Li, A. Jairaman, M. Prakriya, T. Ezponda, D. A. Hildeman, C.-R. Wang, P. T. Schumacker, J. D. Licht, H. Perlman, et al. 2013. Mitochondria are required for antigen-specific T cell activation through reactive oxygen species signaling. *Immunity* 38: 225–236.
30. Yang, Z., H. Fujii, S. V. Mohan, J. J. Goronzy, and C. M. Weyand. 2013. Phosphofructokinase deficiency impairs ATP generation, autophagy, and redox balance in rheumatoid arthritis T cells. *J. Exp. Med.* 210: 2119–2134.
31. Kim, H.-J., and A. E. Nel. 2005. The role of phase II antioxidant enzymes in protecting memory T cells from spontaneous apoptosis in young and old mice. *J. Immunol.* 175: 2948–2959.